

Microbubble Disperse Flow about a Lifting Surface

P.S. Russell¹, J.A. Venning¹, P.A. Brandner¹, B.W. Pearce¹,
D.R. Giosio¹, and S.L. Ceccio²

(¹Australian Maritime College, University of Tasmania, Australia, ²Department of Naval Architecture and Marine Engineering, University of Michigan, USA)

ABSTRACT

The effect of freestream nuclei content on stable cavitation about a hydrofoil and subsequent microbubble production in the wake is investigated experimentally. Microbubble concentrations are measured upstream and downstream of the hydrofoil for four upstream nuclei concentrations and three cavitation numbers. For each case the number of activated nuclei on the hydrofoil and the transverse distribution of concentrations in the wake were measured. Upstream nuclei concentrations were measured with interferometric Mie imaging in the size range between 45-250 μm at concentrations up to 30 cm^{-3} . Wake microbubble concentrations were measured using shadowgraphy in the size range 5-50 μm at concentrations up to 600 cm^{-3} . Wake concentration were found to increase for small changes in low upstream nuclei concentrations but to then decrease for further increase in concentrations. Wake concentrations were found to generally increase with decrease in cavitation number for a particular upstream nuclei concentration. The increase in wake bubble concentrations with seeding increase, at the high cavitation number, is in the smaller bubble size range whereas the increase at the lower cavitation numbers occurs over a greater size range.

INTRODUCTION

Ships are prolific sources of polydisperse bubble populations due to the significant surface disturbances and turbulence they generate. Considerable volumes of air are ingested and dispersed about the hull and by the propulsion and control equipment. Various mechanisms are involved including plunging jets and captured air volumes generated by breaking waves as described by Castro, *et al.* (2014), while surface turbulence may also be sufficient for the hull boundary layer to entrain air (Washuta, *et al.*, 2014; Kim, *et al.*, 2014; Castro, *et al.*, 2016). Lifting surfaces are also of interest here in regards to cavitation occurrence and the consequent contribution to microbubble generation

(Yu & Ceccio, 1997; Russell, *et al.*, 2016). The dynamics of developed cavitation have been recently examined both experimentally (Ganesh, *et al.*, 2016; de Graaf, *et al.*, 2017), and numerically (Gnanaskandan & Mahesh, 2016a,b), however, the mechanisms by which cavitating flows generate microbubbles remain largely to be investigated.

As recently reviewed by Russell, *et al.* (2016) there are limited reported experimental surveys of the bubble distribution within the wake of a cavitating hydrofoil (Maeda, *et al.*, 1991; Yu & Ceccio, 1997; de Graaf, *et al.*, 2014). The results varied slightly with the dominant bubble size found to be of the order of 10 to 40 μm . A spatial survey performed by de Graaf, *et al.* (2014) in the wake of a modified NACA 63A015 hydrofoil ($Re = 6.2 \times 10^5$) found the dominant bubble size to vary in the spanwise and streamwise directions between 25 and 40 μm . A later investigation of the same foil (Russell, *et al.*, 2016) found that for higher Reynolds number the dominant size was 10-25 μm , a result similar to that of Yu & Ceccio (1997).

The role of free stream nuclei in inception continues to be of significant interest in cavitation research as indicated by the following selection of publications from the last three decades (Meyer, *et al.*, 1992; Ran & Katz, 1994; Liu & Brennen, 1998; Gindroz & Billet, 1998; Hsiao & Chahine, 2005; van Rijsbergen & van Terwisga, 2011; Nagaya, *et al.*, 2011; Brandner, *et al.*, 2015; Mørch, 2015; Zhang, *et al.*, 2016; Park & Seong, 2017). As a part of this extensive activity there has been publication also on nuclei measurement techniques, both optical (Lebrun, *et al.*, 2011; Ebert, *et al.*, 2016) and mechanical (Khou, *et al.*, 2016), with a number of studies making comparisons between the various techniques (Billet & Gates, 1981; Katz, *et al.*, 1984; Mées, *et al.*, 2010). As reflected on by Billet (1986), the volume of literature on the topic indicates the complexity of the problem, largely due to its multi-phase and inherently statistical nature. From this it is clear that each of these measurement techniques have their

particular advantages and limitations so that none are indispensable when attempting to extensively examine problems involving the presence of nuclei/microbubbles with both diameters and concentrations ranging over several orders of magnitude. To this end the development of an optical interferometric measurement technique for use in the Cavitation Research Laboratory (CRL) water tunnel at the Australian Maritime College has been established to accompany existing optical (Russell, *et al.*, 2016) and mechanical (Khoo, *et al.*, 2016) bubble measurement capabilities.

Microbubbles respond dynamically to the changing pressure field about a hydrofoil with the effect of uneven diffusion during advection which is still to be fully understood. Not only is the size of the bubble important but the velocity of the bubble relative to that of the surrounding fluid. Given a sufficient velocity difference smaller bubbles can grow from their initial radius by an order of magnitude (Smith & Peterson, 1984). In the context of established cavitation, studies on traveling nuclei bubble cavitation have utilized standard headforms to investigate the dynamics of activated individual bubbles/nuclei (Ceccio & Brennen, 1991; Kuhn, *et al.*, 1995). The maximum radius of activated nuclei is expected to increase as cavitation number decreases. More recently observations have been reported on the significant effect of free stream nuclei content on developed cavitation about a sphere (de Graaf, *et al.*, 2016) and a hydrofoil (Venning, *et al.*, 2017).

The present study follows on and extends the earlier work of Russell, *et al.* (2016) on the measurement of microbubble populations in the wake of a cavitating hydrofoil. A NACA 63A015 profile hydrofoil of similar dimensions to the earlier study has been used. However, a rectangular rather than elliptical profile was selected to achieve a more consistent cavity length over the span of the hydrofoil and achieve a greater spanwise region of nominally uniform bubbly wake. In addition, profiles of microbubble populations were measured across the wake for both the unseeded (background nuclei population only (Venning, *et al.*, 2018)), and a range of three injected nuclei populations. Upstream nuclei populations have been measured using an Interferometric Mie Imaging technique (IMI), individual bubble activations over the hydrofoil surface are obtained from high-resolution still imaging and wake populations characterised via long range microscopy shadowgraphy. From these measurements, observations can be made regarding the effect of upstream nuclei content on the developed cavity dynamics and the resulting microbubble content and distribution in the downstream wake.

EXPERIMENTAL APPROACH

Experiments were carried out in the Cavitation Research Laboratory (CRL) variable pressure water tunnel at the University of Tasmania. The tunnel test section is 0.6 m square by 2.6 m long in which the operating velocity and pressure ranges are 2 to 12 m/s and 4 to 400 kPa absolute, respectively. The tunnel volume is 365 m³, which is filled with demineralised water. The tunnel has ancillary systems for rapid degassing and for continuous injection and removal of nuclei and large volumes of incondensable gas. The test section velocity is measured from one of two (low and high range) Siemens Sitrans P differential pressure transducers models 7MF4433-1DA02-2AB1-Z and 7MF4433-1FA02-2AB1-Z (measuring the calibrated contraction differential pressure) with estimated precision of 0.007 m/s and 0.018 m/s, respectively. The velocity and pressure in the test section are controlled to maintain a constant Reynolds number (Re) and cavitation number (σ). The test section velocity is spatially uniform to within 0.5%, has temporal variations of less than 0.2%, and the free stream turbulence intensity is about 0.5%. Detailed descriptions of the facility are given in Brandner, *et al.* (2006, 2007) and Doolan, *et al.* (2013).

A stainless steel hydrofoil was mounted to the ceiling of the test section, as shown in figure 2, located 1.15 m downstream of the entrance to the test section. The hydrofoil profile was a modified NACA 63A015, rectangular planform hydrofoil, with a chord length of 150 mm (c) and a 300 mm span. The profile modification involved an increase of the trailing edge thickness (see figure 1) to enable practical manufacture of the scaled model and to reduce susceptibility to in-service trailing edge damage. The modified profile was achieved by the addition of $0.00385x$ to the standard profile, where x is the chord-wise distance from the leading edge.

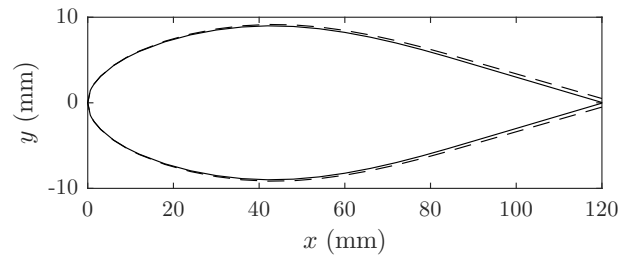


Figure 1: Comparison of a standard (solid) and modified (dashed) NACA 63A015 section. The modification thickens the profile gradually from the leading edge through to a maximum at the trailing edge. Note the aspect is stretched vertically to highlight the difference in profile.

Nuclei were injected from an array of microbubbles generators located in the plenum upstream

of the tunnel honeycomb (figure 2). The array consists of 3 rows of 10 generators distributed on a 80 mm triangular grid which creates a homogeneously seeded nominally rectangular image in the test section enveloping the hydrofoil model (over 300 mm deep by 100 mm wide). The generators used for these experiments are of the so-called minitube type involving the rapid depressurisation of supersaturated water in a confined micro-nozzle the operation of which has been reported on previously (Brandner, *et al.*, 2010; Trump, *et al.*, 2015; Giosio, *et al.*, 2016).

Data was collected using a variety of qualitative and quantitative imaging techniques. Long range microscopy shadowgraphy is a well-established technique for the sizing of particles many times larger than the imaging light wavelength. The technique then can be implemented at many scales but the dynamic range will be dependent on the optical setup (Settles, 2012). Increased magnification will lead to a smaller minimum detectable particle size but will reduce the field of view and depth of field of the system. Therefore increased magnification will reduce the detection volume, the maximum bubble size and increase the number of images for converged statistics. These properties make shadowgraphy well suited for measuring the high bubble concentrations found in the wake of the hydrofoil, typically above $O(10^9) m^{-3}$, but poorly suited for measuring seeding concentration, approx $O(10^4) m^{-3}$ in these experiments.

IMI allows for the sizing of bubbles on the order of microns in size over a much larger field of view than shadowgraphy can accomplish with accurate sizing. However the interference patterns occupy a much larger portion of the sensor than detections in a shadowgraphy image necessitating low volumetric concentrations. The maximum concentrations measurable depends on the illumination used and several other optical parameters particular to the setup (Dehaeck & Van Beeck, 2007; Mées, *et al.*, 2010; Damaschke, *et al.*, 2002) but here can typically measure below $O(10^7) m^{-3}$ with measurable sizes ranging from 50 – 300 μm . This is ideal however for measuring the upstream seeding populations which are both small in size and low in concentration.

Still photography allows us to qualitatively examine the effects seed nuclei have on the cavitation topology but the magnification is such that both seed bubbles and those measured through shadowgraphy are too small to be seen. It appears from these images that the void fraction in the wake increases with increased seeding but what will be investigated here are bubble populations too small in size to be observed in these images.

High-resolution (36.3 megapixel) still photographs of the cavity were captured using a Nikon D810 DSLR with a Nikon AF-S Nikkor 85mm 1:1.4G lens. Illumination was provided by two simultaneously

triggered stroboscopes, a Drello 3018 scope with 4037 flashlamp and a Drello 1018 scope with 4040 flashlamp. Injected nuclei content was measured upstream of the foil using simultaneously acquired in-focus still photography and out-of-focus Interferometric Mie Imaging (IMI), illuminated by a pulsed sheet of Nd-YAG 532 nm laser light oriented along the centerline of the tunnel after passing through a 420–680 nm Thorlabs beam splitting polariser (see figure 3). In focus images were captured by a Nikon D850 DSLR with a Nikkor 105mm lens and were used to collect concentration count statistics and spatially locate the nuclei for later processing of the out-of-focus images. IMI were captured using a Nikon D850 DSLR camera, with a Sigma APO Macro 180 mm F2.8 EX-DG-OS-HSM with the focal plane of the camera positioned 45 mm past the centerline of the tunnel.

Shadowgraphy measurements were taken 5 chord lengths downstream of the hydrofoil midchord, at 1/3 span from the ceiling of the tunnel (or hydrofoil root) for 7 transverse positions when normalised by wake width ($y/w = 0.05, 0.25, 0.40, 0.50, 0.60, 0.75, 0.95$). Shadowgraph images were acquired using a LaVision Imager LX 12-bit 29M camera in combination with a Questar QM100 long-range microscope. The camera CCD sensor size is 6600×4400 pixels. The long-range microscope was coupled to the camera using a $3\times$ Barlow lens giving a field of view of $1917 \mu m \times 1279 \mu m$ with a spatial resolution of $0.29 \mu m/px$. This optical set-up allows a range of bubble sizes from 5 to 300 μm to be measured with a 5 μm bubble being imaged with 17 pixels across the diameter. To improve the optical access the 110 mm acrylic test section side window was replaced by a stainless steel window fitted with a 160 mm diameter 79.5 mm thick glass port. Backlit illumination was provided by a Litron 532 nm 120 mJ 20 Hz Nano L PIV Nd:YAG laser guided through a LaVision high efficiency diffuser using a fluorescent dye plate. A cone of diffused light is produced with emitted pulses in the wavelength range 574 to 580 nm and of 20 ns duration when excited by 5 ns 532 nm laser pulses. Both the camera and diffuser were mounted on a 3-axis Isel (790 mm) linear traverses to allow accurate positioning. The laser and camera were triggered from a programmable timing unit and the acquisition was carried out using LaVision DaVis Version 8.4.0

Data were obtained at a fixed incidence of $\alpha = 3.5^\circ$ for four nuclei seeding concentrations (no seeding, low, high and very high) and three cavitation numbers ($\sigma = 0.35, 0.30, 0.25$) defined by $\sigma = (p - p_v)/0.5\rho U^2$ where p is the freestream static pressure at 1/3 span of the hydrofoil from the ceiling, p_v the vapour pressure, and ρ the density of the fluid. The chord based Reynolds number remained fixed at $Re = Uc/\nu = 1.5 \times 10^6$, where U is the free stream

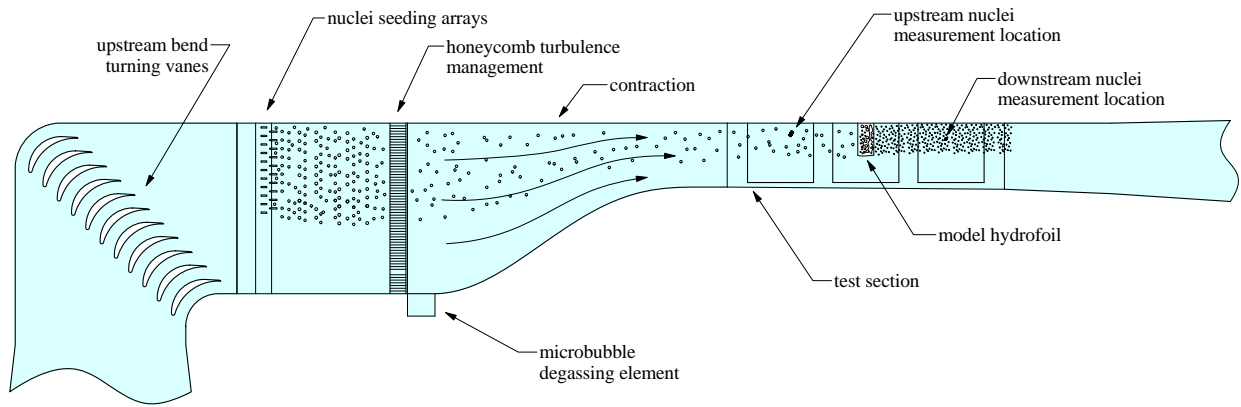


Figure 2: Schematic of microbubble injection and measurement locations within the CRL water tunnel circuit. The optical arrangement used in the water tunnel to detect seeding nuclei through IMI and glare point imaging. The camera on the left captured the interferometric images through a glass port mounted to the wall of the tunnel to ensure optical aberrations are minimised. The camera on the right simultaneously captures in focus glare points for nuclei concentration measurement and the location of the bubbles to be processing with IMI.

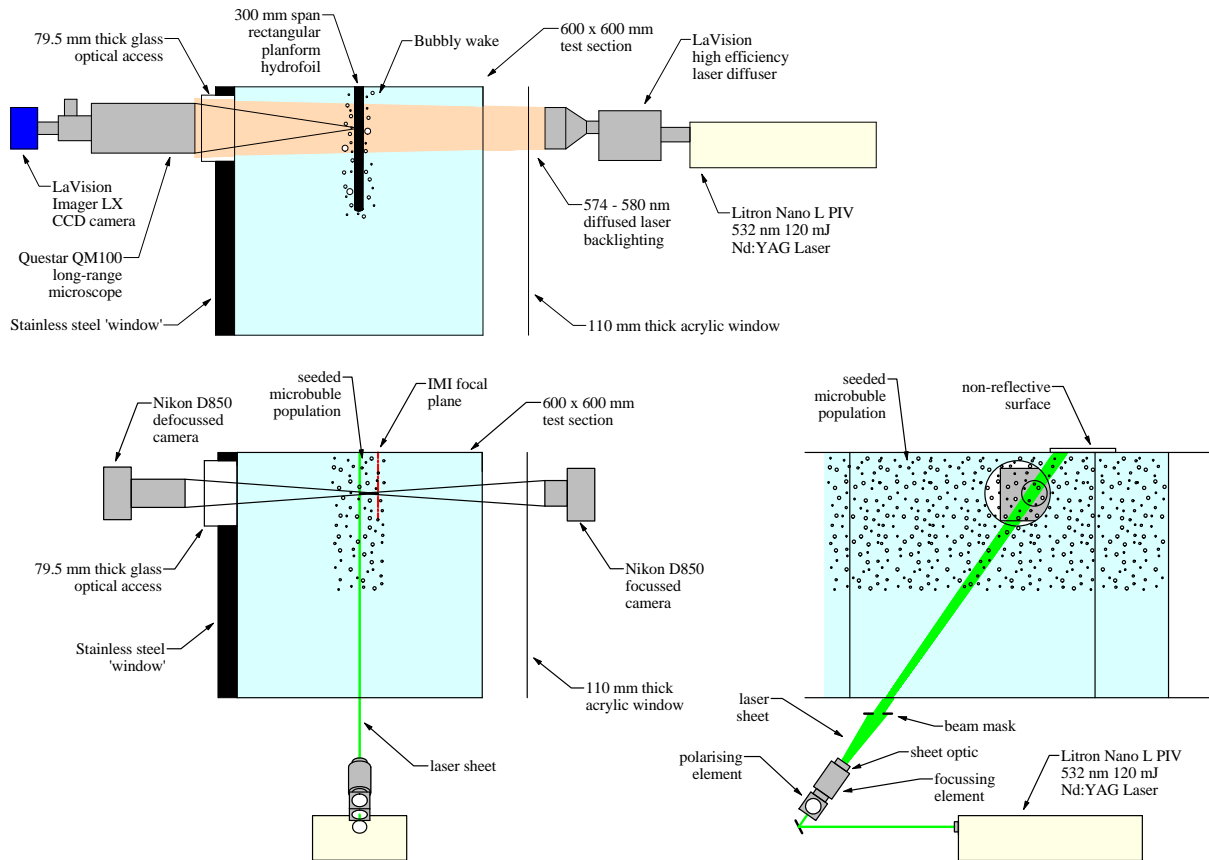


Figure 3: (top) Schematic of experimental set-up for shadowgraphy measurement in the wake of a hydrofoil in the CRL water tunnel test section. (bottom) Schematic of experimental set-up for interferometric nuclei measurement upstream of the foil.

velocity, c the chord length and ν the kinematic viscosity. The dissolved oxygen content was maintained between 2.5-3% for all test conditions. Images showing the range of the conditions tested is presented in figure 4.

All data were processed and analysed in MATLAB 2017a using custom sizing scripts. Shadowgraphy measurements in the wake used localised thresholding to isolate potential bubbles and non-linear multivariate regression to precisely size bubbles with corrections for out of focus blurring. For upstream nuclei measurements the location of nuclei were determined by global thresholding of the in-focus image. A transformation was then applied to these locations to identify the precise center of the bubbles in the out of focus image. A square region containing each out-of-focus pattern was then extracted and analysed using wavelet analysis to measure fringe frequency of the interference lines.

RESULTS

Seeding Measurements

The concentration of injected nuclei was measured by threshold detection from the in-focus glare point images and is summarised in table 1. All tunnel parameters were maintained constant except for the pressure in order to vary the cavitation number. The combined change in pressure and small changes to the operating parameters of the nuclei injectors created changes in the test section nuclei concentration. Lower pressures and thus cavitation numbers were accompanied by an increase in the concentration of nuclei passing the hydrofoil. The aim during testing was to produce four uniformly distributed seeding concentrations. Upon data processing it was clear that the two highest levels of seeding were greatly affected by changes in tunnel pressure and that the middle seeding concentration was higher than anticipated. Interferometric images were able to provide more detail and produced size distributions of the nuclei, see figure 5. It was determined that the minimum size faithfully measured by the system was a microbubble that produced three fringes across its interference pattern. Upon calibration this corresponded to a size of $45 \mu\text{m}$. Background nuclei concentrations in the tunnel have been measured using a cavitation susceptibility meter which show the largest nuclei to be or order $10 \mu\text{m}$ with concentrations of less than 10^{-6} (Venning, *et al.*, 2018). These results imply that the background nuclei concentration from the present IMI measurements are of contaminants only. This is confirmed by inspection of the raw IMI images where detections were found to not show fringe patterns consistent with bubble scattering (Ebert, *et al.*, 2016). These are of such small concentrations that they may be

ignored and have not been corrected for in the seeded measurements. Activation of background nuclei from non-seeded test cases were also not heard during testing or observed in any of the images.

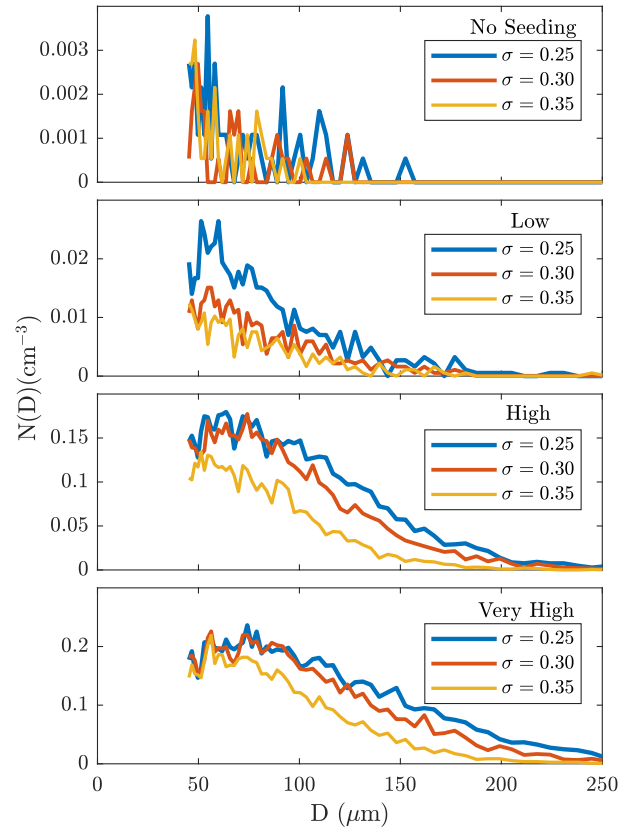


Figure 5: Injected microbubble nuclei distribution measured using IMI upstream of the hydrofoil.

Table 1: Measured seeding concentration per cubic centimeter presented by nominal seeding level and tunnel test section σ values.

(N/cm^3)	$\sigma = 0.35$	$\sigma = 0.30$	$\sigma = 0.25$
No Seeding	0.86	0.71	1
Low	1.77	1.89	2.85
High	14.44	20.9	23.89
Very High	20.1	26.31	31.68

Cavity geometry and topography

A set of high-resolution still photographs (figure 4) provide an overview of the conditions tested. Cavitation about the hydrofoil was tested at a chord based $Re = 1.5 \times 10^6$, and angle of incidence $\alpha = 3.5^\circ$, for a range of seeding concentrations and tunnel σ values.

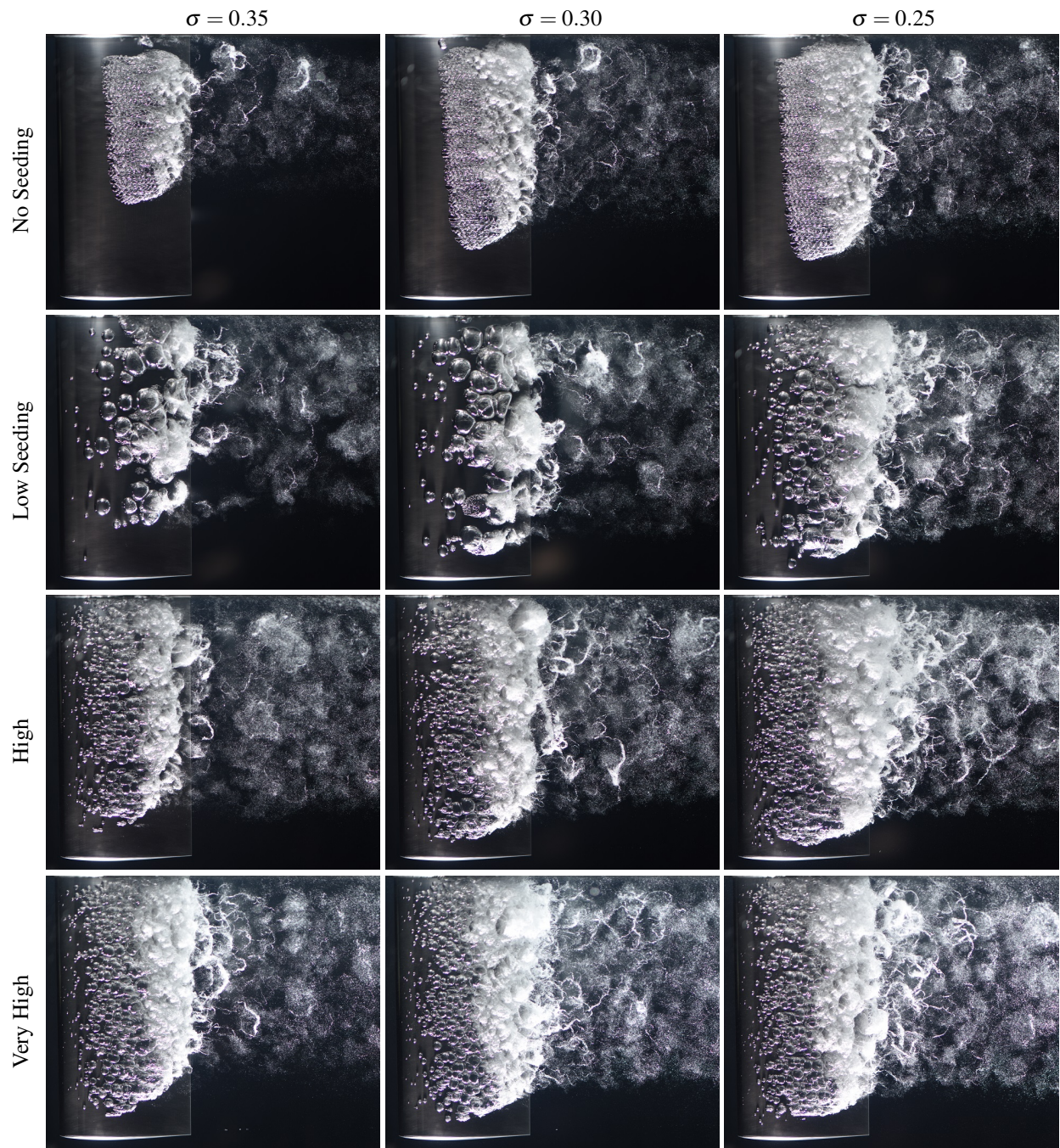


Figure 4: Photographs of the conditions tested. The number of large bubbles in the near wake increased with the concentration of seeding and decreased with cavitation number. Topology of cavity collapse changes with the seed concentration.

Unseeded inception took place just above $\sigma = 0.35$ occurring sooner with the nuclei injection.

Bubbles activated by the foil may undergo fission upon collapse resulting in a cloud of small vapor/gas bubbles when seeding concentrations are sufficiently low (Brennen, 2002). However, bubble-bubble, and bubble-body interactions along with coalescence may modify the cavity closure at higher seeding concentrations (Chahine & Duraiswami, 1992; Takahira, 1997; Hsiao, *et al.*, 2016). The cavity length (streamwise extent) and width (spanwise extent) increased with decreasing σ and increased with seeding level. Primary cavity separation and collapse did not extend beyond the trailing edge of the hydrofoil in all the conditions reported but continued bubble break-up and condensation was observed in the near wake structures. The effect of seeding on the cavity topography may be seen in more detail in figure 6 for fixed $\sigma = 0.35$. Without seeding the leading edge of the cavity has a smooth cellular structure downstream of which interfacial instabilities develop which fed into and affect downstream cavity condensation and breakup (Russell, *et al.*, 2016). Seeded nuclei activated by the hydrofoil immediately broke up the leading edge of the cavity. For low seeding, bubbles activated by the hydrofoil retained their shape longer and grew to larger sizes than at the higher seeding concentrations where greater activation rates led to bubble coalescence and interaction restricting growth. The instability along the cavity surface was no longer able to develop as discrete bubble cavities persisted deep into the breakup region, modifying the collapse physics. The condensation region near the trailing edge was initially reduced with the addition of low levels of seeding but grew larger to exceed the no seeding case as seeding concentrations increased.

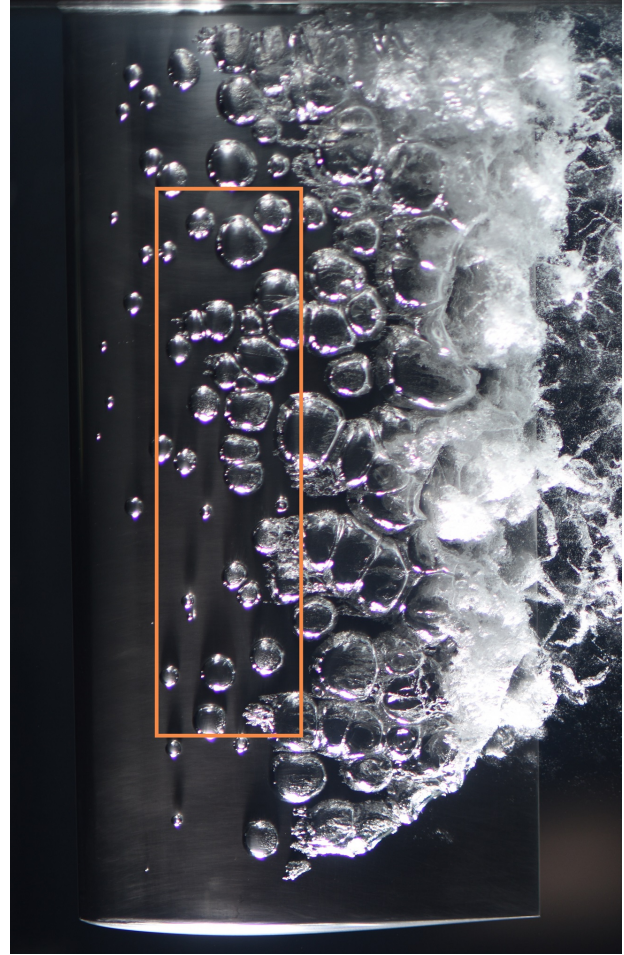


Figure 7: A sample image at tunnel $\sigma = 0.30$ with low nuclei seeding is shown with an overlay highlighting the region of interest (20–50% chord and 20–80% span) in which activated nuclei were counted.

Activated nuclei about the hydrofoil

To explore the effect of seeding further the area concentration of nuclei activated on the hydrofoil between 20–50% chord and 20–80% span at each test condition was measured across 15 images. Figure 7 highlights the region of interest on a sample image. These results are shown in table 2 and plotted in figure 8. The number of activated nuclei shows a sudden increase at low concentrations followed by an apparently linear increase from the low to higher seeded concentrations. For the range of bubble sizes resolved from the IMI (about 50 to 250 μm) there is little static delay suggesting there should be little dependence on nuclei size and cavitation number and that most will be activated with critical pressures about the hydrofoil. The linear trend between upstream concentration and number of activations and the overlap between conditions tends to confirm this observation.

Table 2: Number of bubbles activated between 20–80% span and 20-50% chord of the hydrofoil. (N/cm^2)

μ	$\sigma = 0.35$	$\sigma = 0.30$	$\sigma = 0.25$
No Seeding	0.00	0.00	0.00
Low	0.18	0.29	0.37
High	0.80	1.05	1.06
Very High	1.09	1.20	1.50
Std. Dev	$\sigma = 0.35$	$\sigma = 0.30$	$\sigma = 0.25$
No Seeding	0.00	0.00	0.00
Low	0.04	0.06	0.07
High	0.10	0.09	0.09
Very High	0.12	0.17	0.19

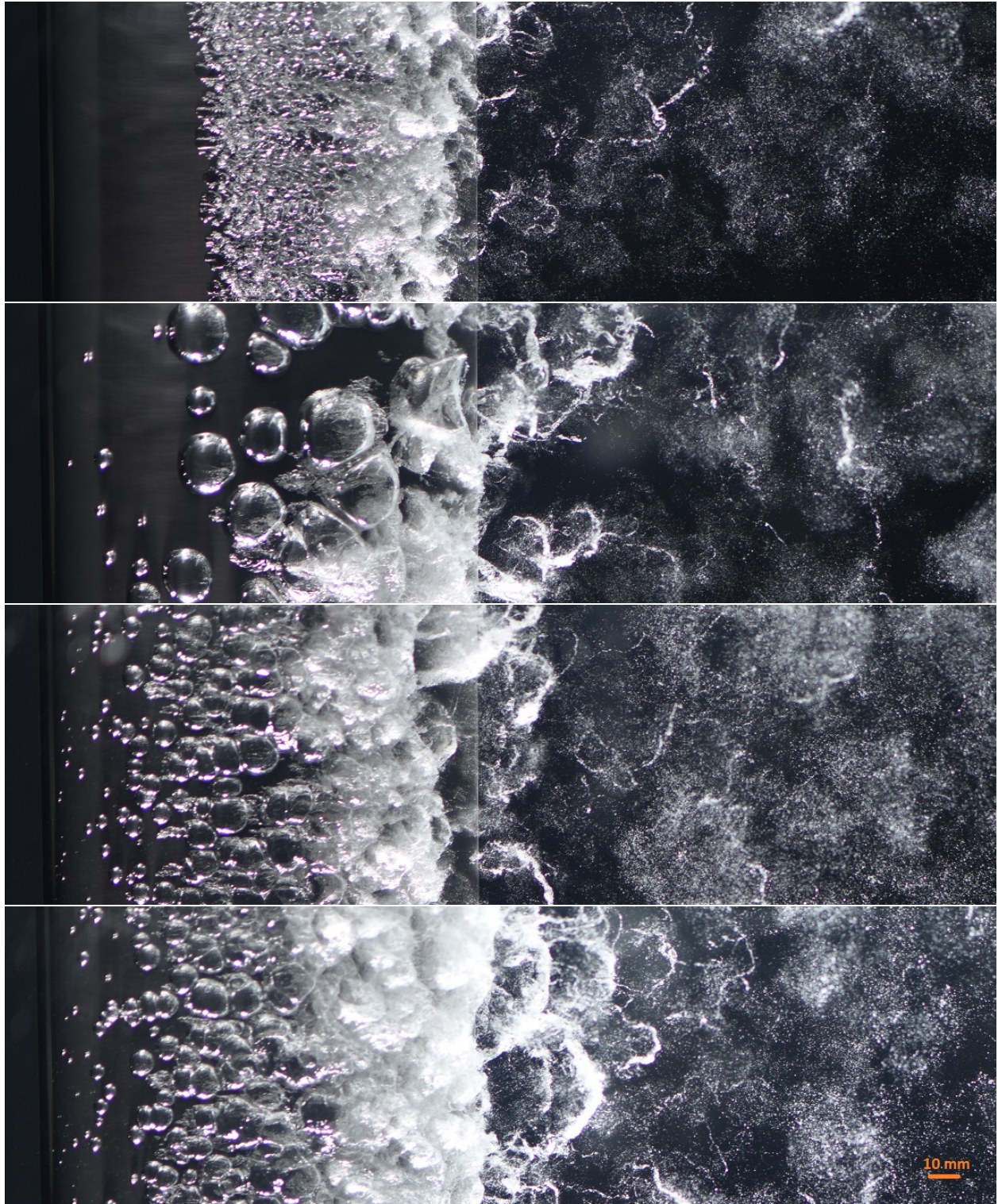


Figure 6: Image samples taken at $\sigma = 0.35$ for the full range of seeding conditions. In all seeded flow cases the stable attached cavity is suppressed. The cavity closure physics changes with seeding concentration. At low seeding level, individual bubble collapse can be observed. At higher seeding, bubbles coalesce into a collapse regime similar to that of an attached cavity but with a higher density of bubbles observed in the wake. Qualitatively, the observed bubble concentration in the wake increases with seeding level.

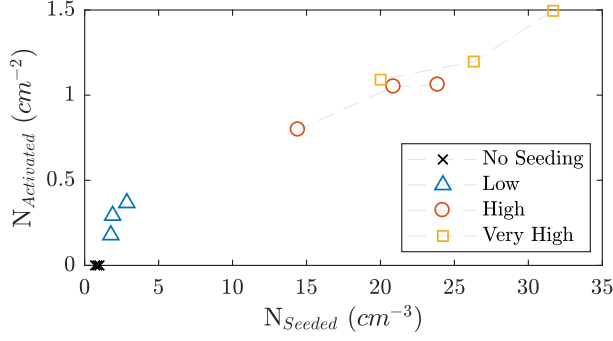


Figure 8: Area concentration of nuclei activations on the hydrofoil for each volumetric concentration injected nuclei.

Shadowgraphy Measurements

The measured spanwise distribution of wake microbubble concentration for each test condition is presented in figure 9. The wake widths varied from about 80 mm wide for the unseeded case to about 100 mm wide for the highest seeding concentration. The pressure and suction sides of the hydrofoil correspond with dimensionless spanwise ordinate $y/w = 0$ and 1 respectively. These results show concentrations within the 0-50 μm size range. Although the measurement system was able to capture bubbles faithfully up to a size of 300 μm inspection of the data revealed that for bubbles larger than 50 μm there were insufficient detections for converged statistics. The shape of these plots indicates a slight asymmetry in the concentration distribution with lower concentrations on the suction side of the wake. Although the peak concentration is generally at about mid wake. The data show a general trend of increasing peak concentration with cavitation number reduction similar to the qualitative trend apparent in the still photography shown in figure 4. The peak concentrations show an increase in the lowest seeding concentration compared with the unseeded case but a slight decrease with further increase in seeding concentration. This effect is most pronounced at low cavitation numbers. These results appear contrary to qualitative observations noted above suggesting that the greater concentrations apparent in figure 4 may be attributable to bubble sizes greater than those measured with the shadowgraphy. This further suggests that two or more magnifications, along with larger data samples, are required to fully resolve the wake microbubble populations. The discrepancy is reconciled by the observation that the intensity of light reflected by bubbles is proportional to their area. This biases the perceived number of bubbles in macro images towards those with larger bubbles. Further, the resolution of the overview image are $\approx 76 \mu\text{m}$ per pixel and so the microbubbles detected through shadowgraphy are smaller

than a single pixel in these macro images. Tests capturing a wider size range at reduced number of transverse locations is planned to examine this further.

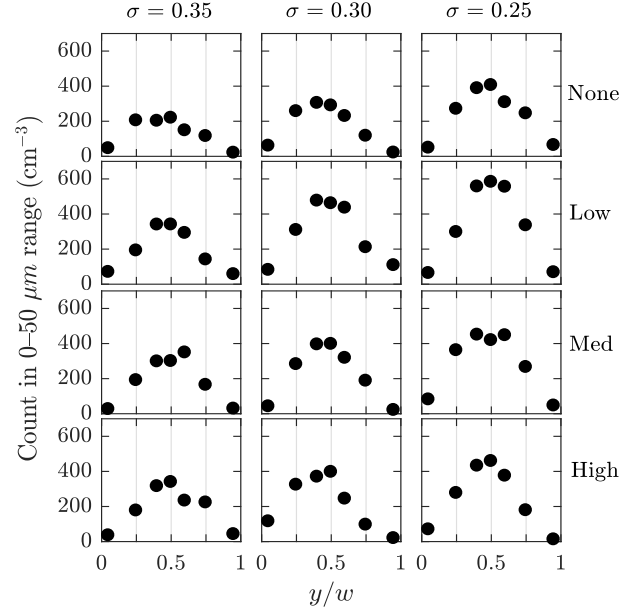


Figure 9: Wake concentrations for bubbles in the 5-50 μm size range are plotted against transverse wake location for each seeding concentration and tunnel cavitation number. A location of 0 corresponds to the edge of the wake on the pressure side of the hydrofoil.

Mean void fraction values from $y/w = 0.4, 0.5, 0.6$, for the measured size range are shown in table 3. These reflect the general trends in concentration discussed above. Similarly the mean concentrations as a function of the area concentration of activations are shown in figure 11 which also reflect the trends discussed above. Overall the results suggest that greater concentrations and increased gas diffusion occurs with lower concentrations where activated bubbles grow to larger sizes than for higher concentrations.

Table 3: Mean void fraction contribution from $y/w = 0.4, 0.5, 0.6$ across the wake for different seeding and σ conditions

Void Fraction $\times 10^{-6}$	$\sigma = 0.35$	$\sigma = 0.30$	$\sigma = 0.25$
No Seeding	9.5	10.7	15.5
Low	13.5	17.3	21.5
High	12.8	14.9	17.8
Very High	13.1	16.9	18.2

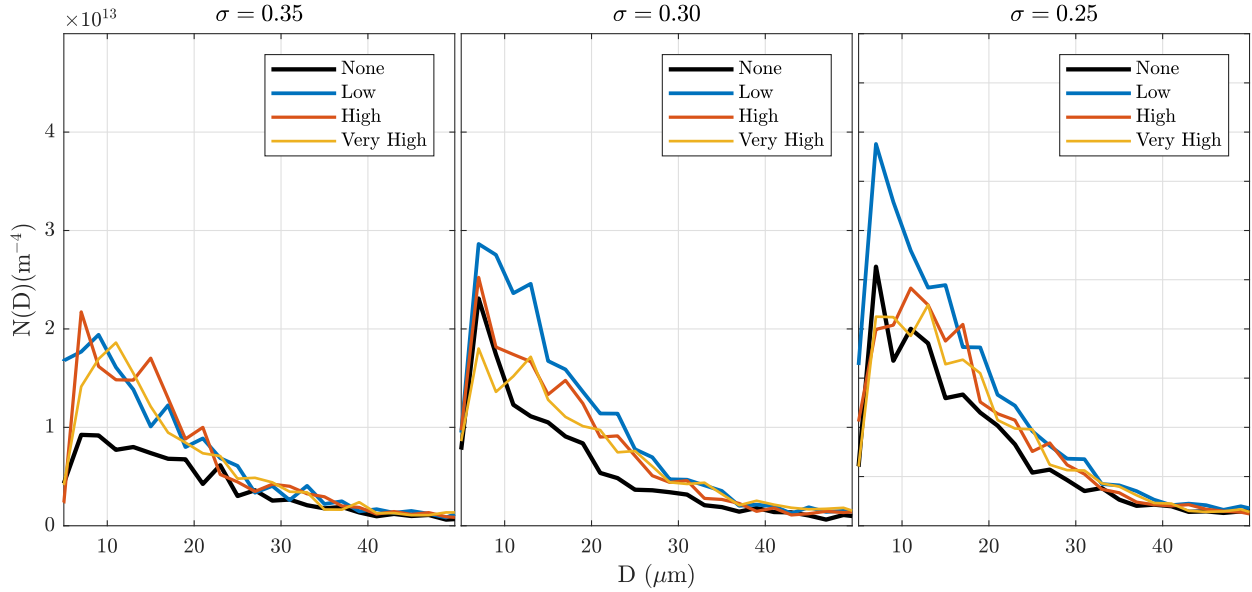


Figure 10: Wake bubble population distributions are plotted for constant tunnel cavitation number at four different seeding levels. An increase in σ resulted in less bubbles. The effect of added nuclei changed with σ , particularly for $\sigma = 0.35$.

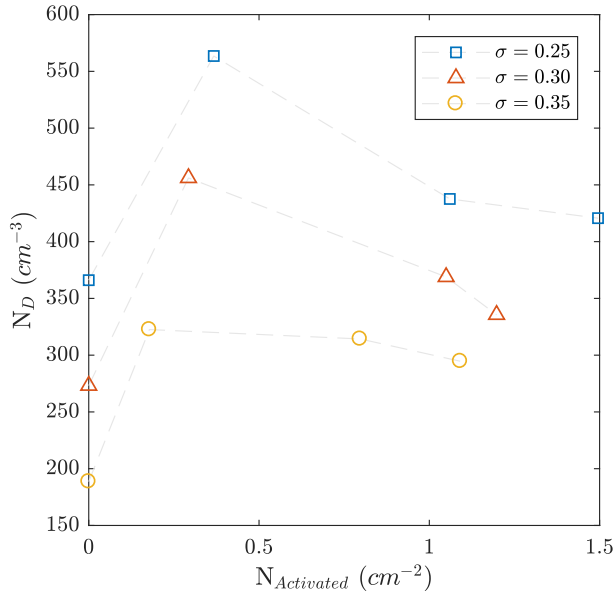


Figure 11: Bubble count per cubic centimeter within the 0-50 μm size range are plotted against the number of nuclei activations per square cm for each seeding line. Whereas, the dashed brown line shows the largest measured wake concentration and tunnel cavitation number.

Mid-wake microbubble population distributions are plotted for each test condition are shown in figure 10. Similar trends are present as with the previous data although differences in the range of bubble sizes affecting these trends can be discerned. For $\sigma = 0.35$,

whilst there is a change in wake concentration with the addition of seeding there is little change with upstream concentration increase. In this case the increase was attributable to bubble sizes in the range below about 22 μm . For the lower cavitation numbers the increase in concentration is attributable to a greater range of bubble sizes. For the low seeding concentration which gave the greatest increase in the wake concentration there is generally a greater increase in the smaller bubble sizes. As discussed further data at lower magnifications are required to improve the dynamic range and fully resolve the total wake populations.

To summarise, the upper and lower bounds of both freestream seeding levels (no seeding and high seeding) and measured wake concentrations are presented in figure 12. The background measurements for the unseeded case were measured using a cavitation susceptibility meter (Venning, *et al.*, 2018), as noted earlier. That is, the dashed blue line is the wake concentration for the unseeded case corresponding to the background concentration shown by the solid blue line. Whereas, the dashed brown line shows the largest measured wake concentration which corresponds to the low seeding level for the lowest $\sigma = 0.25$. The solid black line is for the very high seeding concentration at the lowest $\sigma = 0.25$ which gives a wake concentration between the two dashed lines. These data suggest that the bubble production in the wake is initially highly sensitive to low concentrations but becomes only mildly sensitive to order of magnitude changes in upstream

nuclei concentrations at least within the measurement ranges of the current experiment.

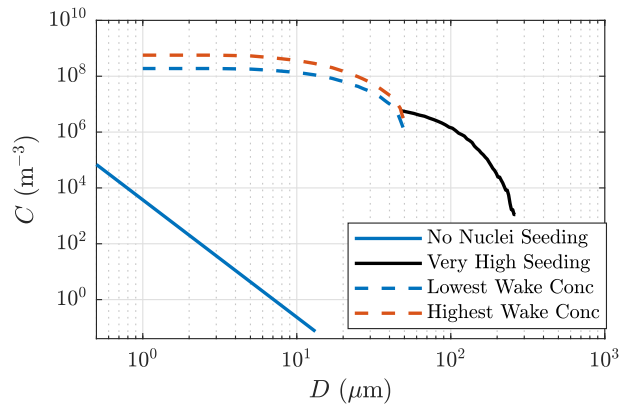


Figure 12: Cumulative populations of the upstream flow (solid lines) and in the wake (dashed, measured with shadowgraphy). The background data for the unseeded case were measured with a cavitation susceptibility meter as reported in Venning, *et al.* (2018).

CONCLUSION

The influence of seeding concentration and cavitation number on the development of cavity geometry and topography, and subsequent microbubble generation has been studied experimentally both qualitatively and quantitatively. The cavity leading edge is broken up by the introduction of freestream nuclei with the condensation and breakup region changing with increased nuclei concentration. Nuclei seeding concentrations were measured and related to the number of activations about the hydrofoil with a portion of the size distributions measured using IMI. High resolution still photography shows that bubble populations increase with nuclei concentrations, however shadowgraphy reveals that microbubble concentration in the range of 5-50 μm increases for low seeding levels but decrease with further increase in seeding concentration. Wake bubble concentrations overall increase with decrease in cavitation number. The increase in wake bubble concentrations with seeding increase, at the high cavitation number, is in the smaller bubble size range whereas the increase at the lower cavitation numbers occurs over a greater size range. Wake microbubble concentrations are highly sensitive to small changes in low active freestream nuclei concentrations but become only mildly sensitive to order of magnitude changes for higher upstream concentrations. Further more extensive measurements using multiple optical setups and with greater sample sizes are required to capture bubbles over a larger range of sizes in the wake to explore these flows further.

ACKNOWLEDGEMENTS

This project was supported by the Defence Science and Technology Group (Mr. Brendon Anderson and Mr. Matthew Khoo), the University of Tasmania, and the US Office of Naval Research (Dr. Ki-Han Kim, Program Officer) and ONR Global (Dr. Pae Wu) through NICOP S&T Grant no. N62909-15-1-2019.

REFERENCES

- Billet, M. L., "Cavitation Nuclei Measurements With an Optical System", *Journal of Fluid Engineering*, Vol. 108, No. 3, 1986, pp. 366–372.
- Billet, M. L., and Gates, E. M., "A Comparison of Two Optical Techniques for Measuring Cavitation Nuclei", *Journal of Fluid Engineering*, Vol. 103, No. 1, 1981, pp. 8–13.
- Brandner, P. A., Lecoffre, Y. and Walker, G.J., "Development of an Australian National Facility for Cavitation Research", *Proceedings of the 6th International Symposium on Cavitation - CAV2006*, 2006, Wageningen, The Netherlands.
- Brandner, P.A., Lecoffre, Y., and Walker, G.J., "Design Considerations in the Development of a Modern Cavitation Tunnel", *Proceedings of the 16th Australasian Fluid Mechanics Conference*, 2007, Gold Coast, QLD, Australia, pp. 630–637.
- Brandner, P.A., Pearce, B.W., and de Graaf, K.L., "Cavitation about a jet in crossflow", *Journal of Fluid Mechanics*, Vol. 768, 2015, pp. 141–174.
- Brandner, P.A., Wright, G., Pearce, B., Goldsworthy, L., and Walker, G.J., "An experimental investigation of microbubble generation in a confined turbulent jet", *Proceedings of the 17th Australasian Fluid Mechanics Conference*, 2010, Auckland, New Zealand.
- Brennen, C.E., "Fission of collapsing cavitation bubbles", *Journal of Fluid Mechanics*, Vol. 472, 2002, pp. 153–166.
- Castro, A.M., Li, J., and Carrica, P.M., "A mechanistic model of bubble entrainment in turbulent free surface flows", *International Journal of Multiphase Flow*, Vol. 86, 2016, pp. 35–55.
- Castro, A.M., Li, J., Hyman, M., and Carrica, P.M., "Turbulent and cavity free surface bubble entrainment with application to ship hydrodynamics", *Proceedings of the 30th Symposium on Naval Hydrodynamics*, 2014, Hobart, Australia.

- Ceccio, S. L., and Brennen, C. E., "Observations of the Dynamics and Acoustics of Travelling Bubble Cavitation", Journal of Fluid Mechanics, Vol. 233, 1991, pp. 633–660.
- Chahine, G.L., and Duraiswami, R., "Dynamical Interactions in a Multi-Bubble Cloud", Journal of Fluids Engineering, Vol. 114, No. 4, 1992, pp. 680–686.
- Damaschke, N., Nobach, H., and Tropea, C., "Optical limits of particle concentration for multi-dimensional particle sizing techniques in fluid mechanics", Experiments in Fluids, Vol. 32, No. 2, 2002, pp. 143–152.
- Doolan, C., Brandner, P.A., Butler, D., Pearce, B., Moreau, D., and Brooks, L., "Hydroacoustic Characterisation of the AMC Cavitation Tunnel", Proceedings of Acoustics 2013 – Science, Technology and Amenity, 2013, Victor Harbor, Australia.
- de Graaf, K.L., Brandner, P. A., and Pearce, B.W., "Spectral content of cloud cavitation about a sphere", Journal of Fluid Mechanics, Vol. 812, 2017, R1.
- de Graaf, K.L., Pearce, B.W., and Brandner, P.A., "The influence of nucleation on cloud cavitation about a sphere", Proceedings of the 16th International Symposium on Transport Phenomena and Dynamics of Rotating Machinery - ISROMAC16, Apr. 2016, Honolulu, Hawaii, USA.
- de Graaf, K.L., Zarruk, G.A., Brandner, P.A., and Pearce, B.W., "Microbubble Content in the Wake of a Cavitating Hydrofoil", Proceedings of the 19th Australasian Fluid Mechanics Conference, Dec. 2014, Melbourne, Australia.
- Dehaeck, S., and Van Beeck, j., "Designing a maximum precision interferometric particle imaging set-up", Experiments in Fluids, Vol. 42, No. 1, 2007, pp. 767–781.
- Ebert, E., Kleinwächter, A., Kostbade, R., and Damaschke, N., "HDNC - Nuclei Size and Number Concentration Estimation with Detection Volume Correction", Proceedings of the 31st Symposium on Naval Hydrodynamics, Sept. 2016, Monterey, California, USA.
- Ganesh, H., Mäkiharju, S.A, and Ceccio, S.L., "Bubbly shock propagation as a mechanism for sheet-to-cloud transition of partial cavities", Journal of Fluid Mechanics, Vol. 802, 2016, pp. 37–78.
- Giosio, D.R., Pearce, B.W., and Brandner, P.A., "Influence of Pressure on Microbubble Production Rate in a Confined Turbulent Jet", Proceedings of the 20th Australasian Fluid Mechanics Conference, Dec. 2016, Perth, Australia.
- Gnanaskandan, A., and Mahesh, K., "Large Eddy Simulation of the transition from sheet to cloud cavitation over a wedge", International Journal of Multiphase Flow, Vol. 83, 2016a, pp. 86–102.
- Gnanaskandan, A., and Mahesh, K., "Numerical investigation of near-wake characteristics of cavitating flow over a circular cylinder", Journal of Fluid Mechanics, Vol. 790, 2016b, pp. 453–491.
- Gindroz, B., and Billet, M.L., "Influence of the Nuclei on the Cavitation Inception for Different Types of Cavitation on Ship Propellers", Journal of Fluids Engineering, Vol. 120, No. 1, 1998, pp. 171–178.
- Hsiao, C.-T., and Chahine, G.L., "Scaling of tip vortex cavitation inception noise with a bubble dynamics model accounting for nuclei size distribution", Journal of Fluids Engineering, Vol. 127, No. 1, 2005, pp. 55–65.
- Hsiao, C.-T., Ma, J., and Chahine, G.L., "Numerical Study of Bubble Cloud Dynamics near a Rigid Wall", Proceedings of the 31nd Symposium on Naval Hydrodynamics, Sept. 2016, Monterey, CA, USA.
- Katz, J., Gowing, S., O'Hern, T., and Acosta, A., "A Comparative Study Between Holographic and Light-Scattering Techniques of Microbubble Detection", in Measuring Techniques in Gas-Liquid Two-Phase Flows, Springer, Berlin, Heidelberg, 1984, pp. 41–66.
- Khoo, M.T., Venning, J.A., Pearce, B.W., Brandner, P.A., and Lecoffre, Y., "Development of a Cavitation Susceptibility Meter for Nuclei Size Distribution Measurements", Proceedings of the 20th Australasian Fluid Mechanics Conference, Dec. 2016, Perth, Australia.
- Kim, D., Mani, A., and Moin, P., "Investigation of bubble formation by breaking waves in turbulent two-phase Couette flows", Proceedings of the 30th Symposium on Naval Hydrodynamics, Nov. 2014, Hobart, Australia.
- Kuhn de Chizelle, Y., Ceccio, S. L., and Brennen, C. E., "Observations and Scaling of Travelling Bubble

- Cavitation”, Journal of Fluid Mechanics, Vol. 293, 1995, pp. 99–126.
- Lebrun, D., Allano, D., Méés, L., Walle, F., Corbin, F., Boucheron, R., and Fréchou, D., ”Size measurement of bubbles in a cavitation tunnel by digital in-line holography”, Applied Optics, Vol. 50, No. 34, 2011, pp. H1–H9.
- Liu, Z., and Brennen, C. E., ”Cavitation nuclei population and event rates”, Journal of Fluids Engineering, Vol. 120, No. 4, Dec 1998, pp. 728–737.
- Maeda, M., Yamaguchi, H., and Kato, H., ”Laser holography measurement of bubble population in cavitation cloud on a foil section”, Proceedings of the 1st ASME-JSME Fluids Engineering Conference, 1991, Portland, OR, pp. 23–27.
- Méés, L., Lebrun, D., Allano, D., Walle, F., Lecoffre, Y., Boucheron, R., and Fréchou, D., ”Development of interferometric techniques for nuclei size measurement in cavitation tunnel”, in Proceedings of the 28th Symposium on Naval Hydrodynamics, Sept. 2010, Pasadena, California, USA.
- Meyer, R. S., Billet, M. L., and Holl, J. W., ”Freestream Nuclei and Travelling Bubble Cavitation”, Journal of Fluids Engineering, Vol. 144, No. 4, 1992, pp. 672–679.
- Mørch, K.A., ”Cavitation inception from bubble nuclei”, Interface Focus, Vol. 5, No. 5, 2015, pp. 20150006.
- Nagaya, S., Kimoto, R., Naganuma, K., and Mori, T., ”Observation and scaling of tip vortex cavitation on elliptical hydrofoils”, in Proceedings of the ASME-JSME-KSME Joint Fluids Engineering Conference, Hamamatsu, Japan, 2011, paper AJK2011-33015, pp. 225–230.
- Park, J., and Seong, W., ”Experimental Study on the Effect of Number of Bubble Occurrences on Tip Vortex Cavitation Noise Scaling Law”, Journal of Fluids Engineering, Vol. 139, No. 6, 2017, pp. 061303.
- Ran, B., and Katz, J., ”Pressure fluctuations and their effect on cavitation inception within water jets”, Journal of Fluid Mechanics, Vol. 262, 1994, pp. 223–263.
- Russell, P.S., Giosio, D.R., Venning, .A., Pearce, B.W., Brandner, P.A., and Ceccio, S.L., ”Microbubble generation from condensation and turbulent breakup of sheet cavitation,” Proceedings of the 31th Symposium on Naval Hydrodynamics, Sept. 2016, Monterey, California, USA.
- Settles, G.S., ”Schlieren and shadowgraph techniques: visualizing phenomena in transparent media”, Springer Science & Business Media, 2012.
- Smith, R.W., and Peterson, R.S., ”Dynamic and diffusive growth of microbubbles near a two-dimensional hydrofoil”, IEEE Journal of Oceanic Engineering, Vol. 9, No. 2, 1984, pp. 93-97.
- Takahira, H., ”Growth of traveling bubbles near an axisymmetric body in a potential flow”, JSME International Journal, Series B, Fluids and Thermal Engineering, Vol. 40, No. 2, 1997, pp. 240–249.
- Trump, M.C., de Graaf, K.L., Pearce, B.W., and Brandner, P.A., ”An Experimental Investigation of the Optical Measurement of Microbubbles in a Confined Radial Jet”, Proceedings of the 4th Australian Conference on Laser Diagnostics in Fluid Mechanics and Combustion, Dec. 2015, Melbourne, Australia, pp. 29–34.
- van Rijsbergen, M., and van Terwisga, T., ”High-speed micro-scale observations of nuclei-induced sheet cavitation”, Proceedings of the WIMRC FORUM 2011 on Cavitation: Turbo-machinery & Medical Applications, July 2011, University of Warwick, UK, pp. 225–230.
- Venning, J.A., Khoo, M.T., Pearce, B.W., and Brandner, P.A., ”Background nuclei measurements and implications for cavitation inception in hydrodynamic test facilities”, Experiments in Fluids, Accepted for publication , 2018.
- Venning, J., Smith, S., Brandner, P., Giosio, D., and Pearce, B., ”The influence of nuclei content on cloud cavitation about a hydrofoil”, Proceedings of the 17th International Symposium on Transport Phenomena and Dynamics of Rotating Machinery - ISROMAC17, Dec. 2017, Maui, Hawaii, USA.
- Washuta, N., Masnadi, N., and Duncan, J., ”The turbulent boundary layer on a horizontally moving partially submerged, surface-piercing vertical wall”, Proceedings of the 30th Symposium on Naval Hydrodynamics, Nov. 2014, Hobart, Australia.
- Yu, P.-W., and Ceccio, S.L., ”Diffusion induced bubble populations downstream of a partial cavity”, Journal of Fluids Engineering, Vol. 119, No. 4, 1997, pp. 782–787.
- Zhang, L., Chen, L. and Shao, X., ”The migration and growth of nuclei in an ideal vortex flow”, Physics of Fluids, Vol. 28, No. 12, 2016, pp. 123305.